Probabilistic Northern Hemisphere Freeze/Thaw Data Record derived from Satellite Multi-Frequency Microwave Brightness Temperatures

Beta Release

Contact Information:
Kellen Donahue, Jinyang Du, Tobias Kundig, and John S. Kimball
Numerical Terradynamic Simulation Group (NTSG)
The University of Montana
Missoula MT, 59812
Email: johnk@ntsg.umt.edu; jinyang.du@umontana.edu, tobias.kundig@mso.umt.edu; kellen.donahue@umconnect.umt.edu.

Project URL: http://freezethaw.ntsg.umt.edu

Release date: 2022-06-15

Acknowledgements: These data were generated through a grant from the NASA MEaSUREs (Making Earth System Data Records for Use in Research Environments) program (80NSSC18K0980). This work was conducted at the University of Montana under contract to NASA.

Contents:

1 - INTRODUCTION

This document provides information relating to a probabilistic Northern Hemisphere freeze/thaw (FT) data record derived using a U-Net neural network architecture informed by satellite multi-frequency microwave brightness temperature retrievals from the NASA SMAP (Soil Moisture Active Passive) and JAXA AMSR2 (Advanced Microwave Scanning Radiometer 2) radiometers. Unlike other available FT data records that provide only a binary (0,1) classification of frozen or non-frozen conditions, this product includes both binary FT and continuous variable estimates of the probability of thawed conditions. This product is designed to complement other established binary FT data records, including the NASA FT Earth System Data Record (Kim et al. 2021) and SMAP Level 3 FT operational products (Xu et al. 2020), by providing a probabilistic FT variable with enhanced accuracy and sensitivity to surface soil FT conditions.

The biophysical importance of the FT retrieval from satellite microwave remote sensing is well established, providing an effective proxy of the timing, extent and duration of frozen conditions in the landscape (McDonald and Kimball 2005). Over half (~66 million km^2) of the global land area experiences seasonal FT processes profoundly affecting surface meteorology and hydrologic activity, vegetation productivity and ecological trace gas dynamics (Kim, Kimball, and Du 2017). Microwave sensors are uniquely capable of detecting and monitoring FT status owing to their strong sensitivity to changes in the relative abundance of liquid water as the landscape transitions between predominantly frozen and thawed states. The lower frequency (~ ≤ K_u-band) measurements available from many operational polar-orbiting satellites are also insensitive to solar illumination

and atmospheric contamination, enabling consistent, near-daily observations day-or-night and under nearly all-weather conditions.

This Beta Release product is intended for research purposes and should be used with caution pending further testing and final publication of the model algorithms and product performance. Future product releases may include refinements to the data format, model algorithms and inputs, spatial and temporal coverage of the data record, and documentation.

2 - Data Description

This daily data record includes both binary and probabilistic FT variables produced using the same U-Net neural network and geospatial inputs. The model inputs include: rSIR spatially enhanced vertically and horizontally polarized brightness temperatures (T_Bs) from SMAP (1.4 GHz) (Brown and Long 2022) and overlapping AMSR2 (18.7 Ghz and 37 GHz) T_B retrievals mapped to a consistent global grid (JAXA). The T_B retrievals include both ascending (6am SMAP; 1:30pm AMSR2) and descending (6am SMAP; 1:30am AMSR2) local orbital overpass sampling times. Additional model inputs include Global Multi-Resolution Terrain Elevation Data (GMTED2010) and latitude. The product contains daily local morning (6am) and evening (6pm) FT predictions spanning the data years from 2016 through 2020. The beginning of the data record is defined by the first complete calendar year of SMAP observations, while future extensions to the data record are enabled from ongoing overlapping SMAP and AMSR operations. All model inputs and outputs are formatted to the Northern Hemisphere Polar EASE-Grid 2 projection (Mary J. Brodzik et al. 2014) consistent with the Polar Enhanced Resolution (PER) ESDR and SMAP FT records (Kim et al. 2021; Xu et al. 2020). The 9-km product grid resolution is also consistent with the resolution of the rSIR T_B inputs and the SMAP enhanced L3 radiometer Northern Hemisphere FT product (Xu et al. 2020).

This product is intended to provide a reliable FT classification for all non-permanently frozen lands in the Northern Hemisphere, along with enhanced spatial information, accuracy, and soil FT sensitivity gained from the use of complimentary multi-frequency T_B inputs. The combined use of SMAP L-band (1.4 GHz) T_B observations and AMSR2 higher frequency T_B retrievals as key inputs to a U-Net machine learning model trained using soil FT observations from both model reanalysis and in situ soil temperature network measurements is expected to provide enhanced product sensitivity to FT conditions in the surface soil layer. The resulting product includes a continuous variable estimate of the probability of thawed conditions, which may have enhanced information and utility for some applications (Farhadi et al. 2015; Zwieback et al. 2011).

An example of the product outputs showing the probability of frozen conditions for four selected days in 2016 is shown in **Figure 1**. The U-Net model outputs and associated product includes a daily binary FT classification (0 for frozen, 1 for thawed) for all land on a 9km polar grid, along with a continuous FT classification ranging from low (0) to high (1) probability of thawed conditions on the same grid. Masked grid cells (e.g. black areas in Fig. 1) include cells dominated by open water, permanent Ice cover, or permanently frozen land as defined by the EASE-Grid Land-Ocean-Coastline-Ice Masks (M. J. Brodzik and NSIDC, 2013). The model is trained from independent temperature observations to recognize and classify FT transitions across the 0ºC thermal boundary between predominantly frozen and thawed ground conditions. Here, the model inputs are sensitive to the large characteristic T_B response to changes in near-surface liquid water abundance and associated dielectric properties that occur during landscape FT transitions. The combined use of different frequencies and polarizations provide additional information to better distinguish soil FT transitions from other landscape FT contributions from lower atmosphere, snow and vegetation components of the sensor footprint. The product includes different daily fields for local morning and afternoon FT conditions, which are derived from similarly trained but separate models using ascending and descending overpass T_B inputs.

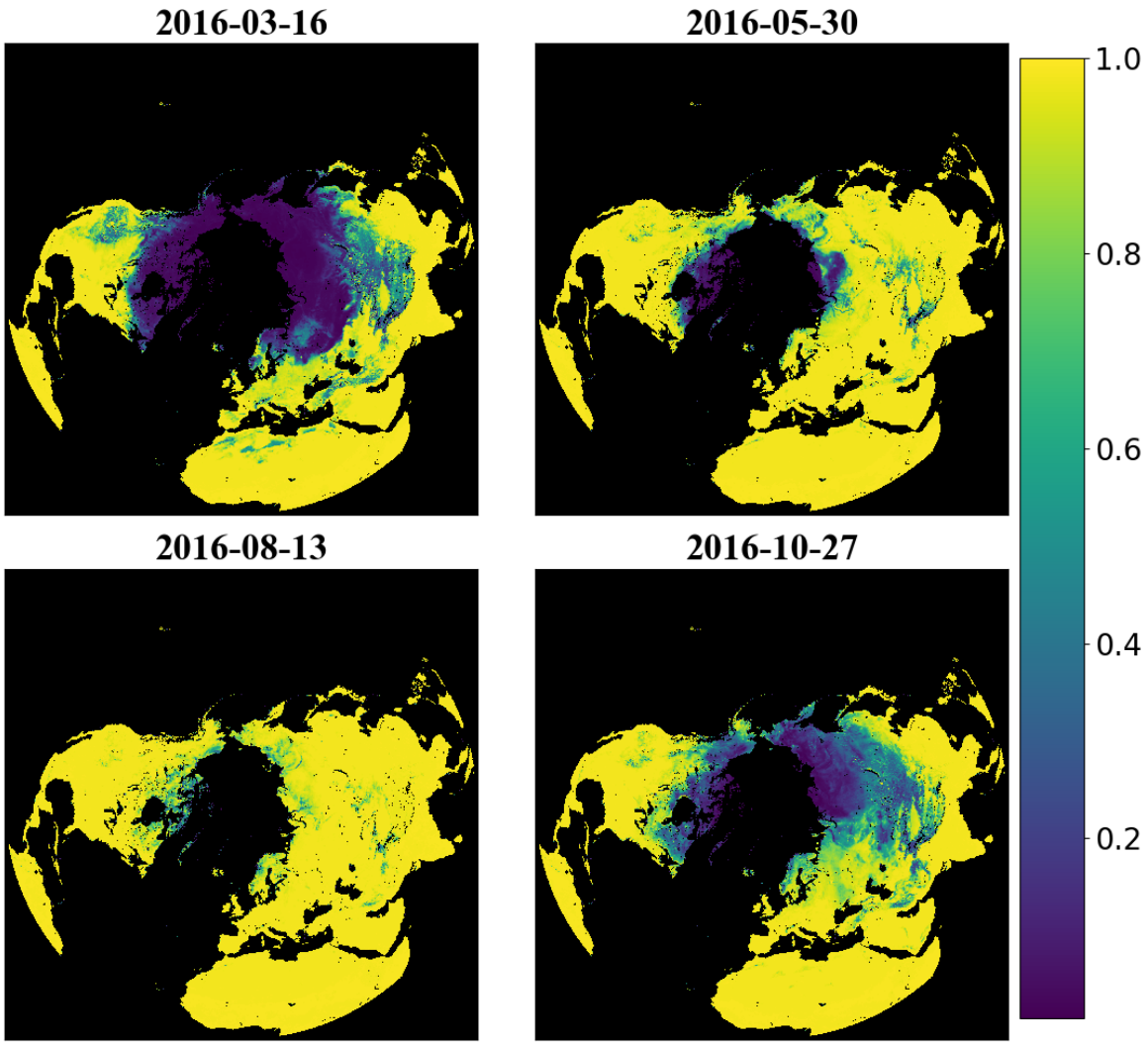

***Figure 1**: Example product fields showing the probability of thawed conditions for four selected days over the 2016 seasonal cycle. The probability of thawed conditions ranges from low (0) to high (1) and is lower at higher latitudes and upper elevations during early spring (Mar) and late fall (Oct) in the Northern Hemisphere; in contrast, the probability of thawed conditions is much greater during mid-summer (Aug).*

3 - Accuracy and performance

The product was validated using a combination of in-situ topsoil (≤5cm depth) temperature measurements from the Northern Hemisphere weather station network and ERA5 Reanalysis surface layer (Layer 1) soil temperature data. The in-situ soil temperature measurements were used for the primary validation, but were supplemented with ERA5 temperatures to compensate for the sparse weather station network (***Figure 3***). The daily temperature records were converted to FT prior to the

validation assessment using a 0ºC threshold to distinguish between frozen and non-frozen conditions. The morning and afternoon FT product fields were then compared against the respective 6am and 6pm readings of the temperature observations. These times were selected to represent diurnal conditions more likely to be uniform in soil temperature and soil dielectric properties, while also matching the SMAP orbital overpass times.

A summary of the product accuracy for a selected data year (2016) is shown in **Table 1**. The overall product accuracy for the morning (6am) FT data is 93.1% when compared to ERA5 and 92.5% compared to the in situ soil temperature measurements. The relative accuracy varies seasonally, ranging from 98.7% in the summer months to 89.6% in the winter months. The product also shows variable performance in different regions, as shown relative to ERA5 (***Figure 2***) and in-situ weather station (***Figure 3***) soil temperature records. The relative product accuracy is generally lower over complex mountain terrain such as the Rocky Mountains and Himalayas due to the scale mismatch between the relatively coarse satellite T_B measurement footprint relative to the larger FT heterogeneity driven by the complex topography. The product accuracy is also lower over the Tibetan Plateau, where the complex terrain and arid landscape may reduce the effective microwave FT signal. Despite the above limitations, the product performance is similar or better than the accuracy reported from other available FT products from SMAP and the ESDR baseline (Kim et al. 2017; Derksen et al. 2017; Kim et al. 2019).

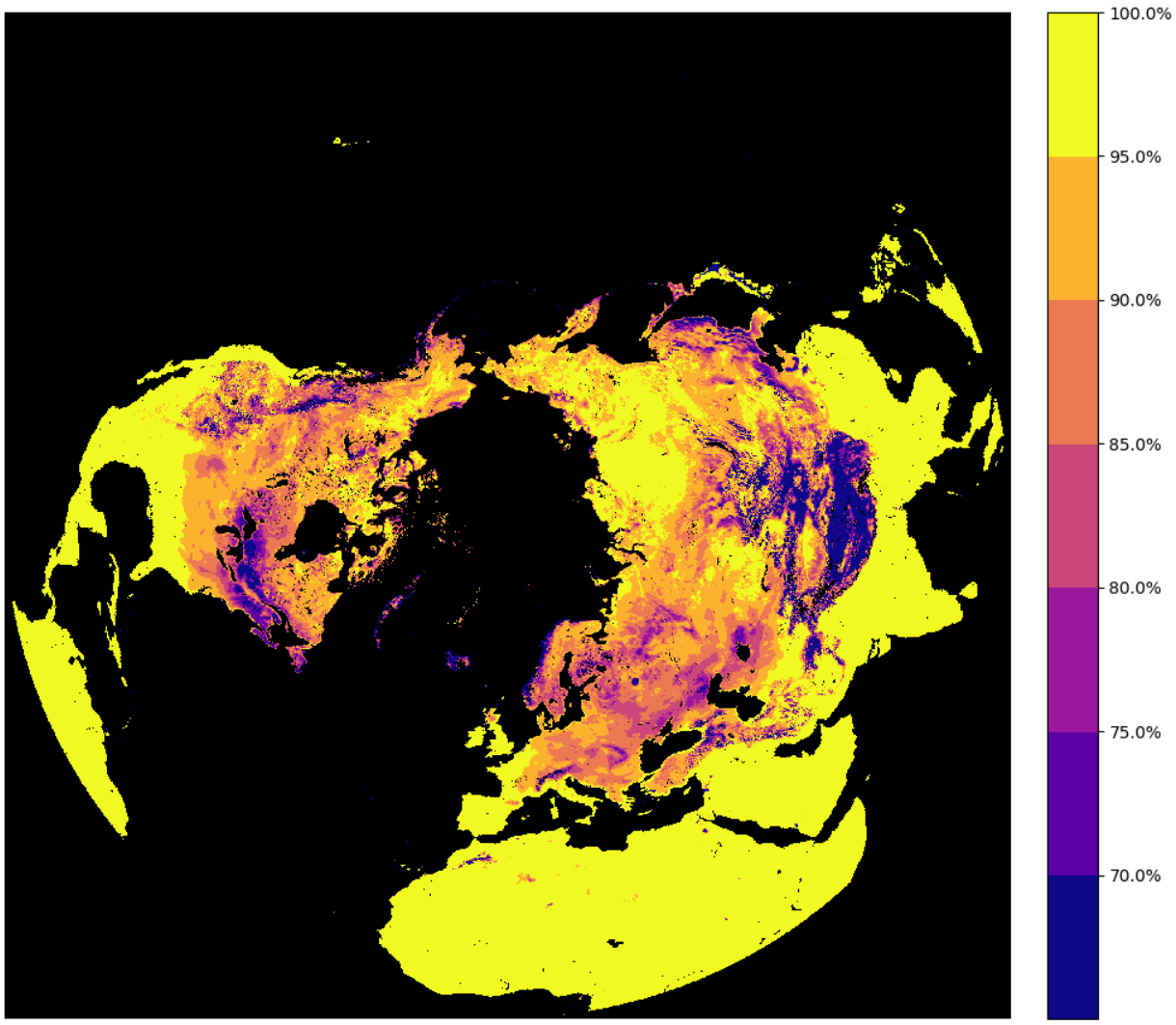

Figure 2: *Mean percent accuracy of the product in relation to ERA5 temperature based FT data for selected data year 2016. Black areas denote masked regions outside of the product domain.*

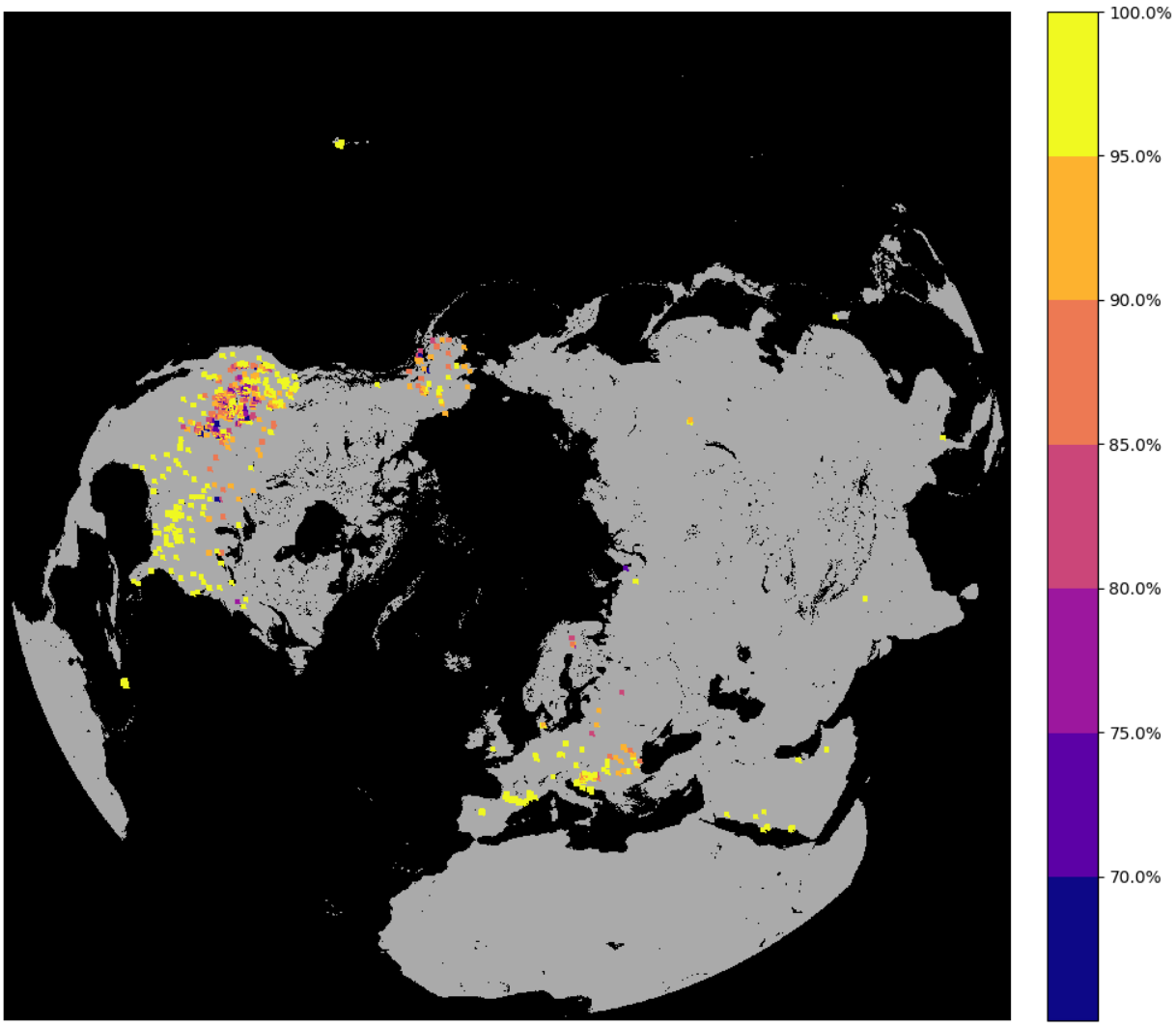

Figure 3: *Mean percent accuracy of the product in relation to soil temperature measurement based FT data from the regional weather station network for selected data year 2016. 728 stations were used in the validation assessment. Black areas denote masked regions outside of the product domain.*

4 - Ancillary Data used for Model Inputs and Training

The SMAP T_B record used to derive the FT product was obtained from the SMAP rSIR enhanced grid product (Brodzik et al., 2021), which is provided in a 9km polar EASE-grid 2 projection consistent with the FT product format and with spatially enhanced gridding and favorable performance relative to the SMAP native (~40-km) T_B sampling footprint (Brown and Long, 2022). Land recordings occur at approximately two-day intervals for land areas above 45ºN, with consistent 6pm/am local

ascending/descending orbital overpass sampling times for the vertical and horizontal polarization T_B retrievals. The SMAP rSIR period of record used for processing begins March 31, 2015 and extended to May 1, 2021 at the time of this study. To construct complete daily records for each morning and afternoon T_B time series, missing T_B data between satellite swathes were gap-filled using a weighted average between the two most recent adjacent retrievals within up to a five-day moving window, as:

$$T_{missing} = T_{prev} * (1 - \frac{D_{prev}}{D_{prev}+D_{next}}) + T_{next} * (1 - \frac{D_{next}}{D_{prev}+D_{next}}) \quad (1)$$

In the above equation, $T_{missing}$ is the missing data being filled at a given location and time step, T_{prev} is the most recent valid data before a missing data value in the time series; T_{next} is the most recent data after the missing data value, D_{prev} is the number of days between $T_{missing}$ and T_{prev}, and D_{next} is the number of days between $T_{missing}$ and T_{next}. If no T_B data is present in the five-day window then the pixel is masked out to prevent gaps from being filled with data too temporally distant.

The AMSR2 T_B data was obtained for the 18.7 GHz and 36.5 GHz channels and vertical and horizontal polarizations overlapping with the same period of record as SMAP. The AMSR2 data were obtained in a consistent 10 km resolution global EASE-grid format from the AMSR2 GCOM-W Level3 product available through the JAXA G-Portal. The AMSR2 T_B retrievals include twice-daily coverage at higher latitudes owing to a relatively wide sensor swath and consistent 1:30am/pm local sampling from the orbital swath retrievals. Missing data was gap-filled in the same manner as the SMAP data (above). The AMSR2 data was then reprojected to the 9km polar EASE-grid 2 format using the LinearNDInterpolator from the scipy package. A linear interpolation method was chosen to provide a smooth reprojection of the data that considers all nearby cells when calculating the values for the grid.

We used in-situ soil temperature measurements from available Northern Hemisphere station networks, including the Water and Climate Information System (USDA Natural Resources Conservation Service, 2017), International Soil Moisture Network (Dorigo et al., 2021; Musial et al., 2016; Ikonen et al., n.d.; Wigneron et al., 2018; Vreugdenhil et al., 2013; Bircher et al., 2012; Beyrich and Adam, 2007; González-Zamora et al., 2019; “ASSIMO Project” n.d.; Calvet et al., 2007; Bogena et al., 2012; Petropoulos and McCalmont, 2017; “NVE” n.d.; Varlagin, n.d.), Global Terrestrial Network for Permafrost (GTN-P 2015), and GLOBE (“Global Learning and Observations to Benefit the Environment (GLOBE) Program” n.d.). The distribution of stations for the selected year 2016 is shown in **Figure 4**. For each station location, we only used the shallowest soil temperature readings (within 5 cm depth) with local measurements obtained as close as

possible to the 6am and 6pm SMAP sampling times. The location of each station measurement was assigned to the nearest grid cell in the 9km polar EASE-grid. If multiple stations were assigned to the same grid cell then the associated temperatures were averaged to produce the bulk value of the cell at each time step. The morning and afternoon temperature measurements were then classified into FT categories using a 0ºC FT threshold.

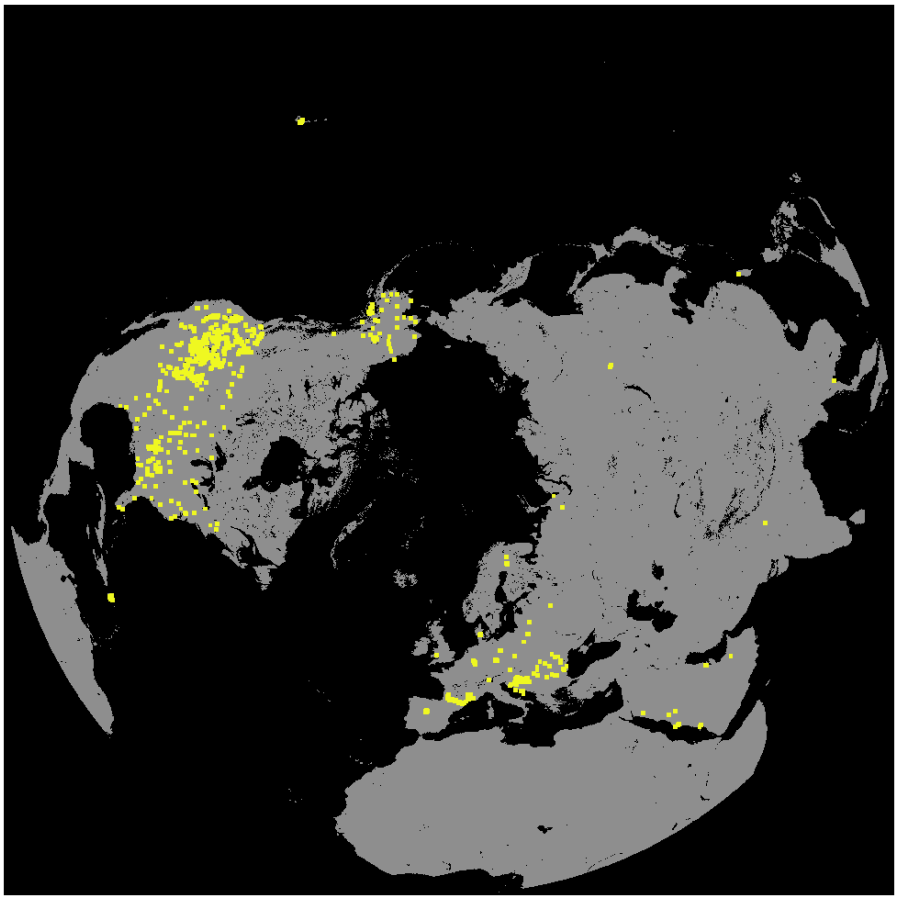

Figure 4: *Map of weather station locations with in situ soil temperature measurements for the year 2016. A total of 728 stations are represented.*

The station temperature measurements reflect actual ground conditions useful for model validation, but the stations lack consistent sampling and are sparsely located. The actual number of station measurements also varies over time or may not be representative of the coarser model and satellite footprints, which can introduce uncertainty. To compensate for the limitations of the sparse station measurement network we also included daily surface layer temperatures from ECMWF ERA5 global reanalysis data. ERA5 is a state-of-the-art model and data reanalysis product produced

in a global 30 km resolution and hourly time step (Hersbach et al., 2020). For this study we used the ERA5 daily 6am and 6pm surface temperature (Layer 1) readings. The ERA5 temperature data was reprojected to the 9 km polar EASE-grid 2 projection using the same method as the AMSR2 data. ERA5 temperatures were also converted to FT values using the same procedure as was used for the in situ temperature processing. Because ERA5 is still a model output instead of a direct measurement, we put more weight on the station temperature measurements for the product validation, although the station measurements also have limitations as noted above.

5 – U-Net Architecture

The U-Net architecture used for the product has a depth of 4 downscaling and 4 upscaling layers with an initial filter bank size of 32 channels (**Figure 5**). U-Net and its variants are highly effective for image segmentation and have been applied to biomedical (Ronneberger et al., 2015; Qamar et al., 2020) and satellite (Ulmas and Liiv, 2020; McGlinchy et al., 2019) imagery which makes them an ideal candidate for segmenting FT regions. U-Net works by first running the inputs through multiple steps of convolutional blocks followed by max pool downsampling operations. This procedure condenses the amount of spatial information while increasing feature information. The process is then reversed with transposed convolution upsampling operations followed by convolutional blocks to take the condensed feature information and use it to construct the high resolution segmented output. After each upsampling process, the corresponding downsampling information is concatenated through a skip connection to reintroduce the original spatial information to the data. Each convolutional block contains two sequences of a 3x3 convolution followed by a 2d batch normalization and a leaky ReLU activation function. The primary difference in our model to the standard U-Net is the inclusion of spatial dropout layers at the end of each convolutional block with a dropout rate of 20% (Tompson et al., 2014). Dropout is used alongside a strong L2 weight normalization of 1e-3 to prevent over saturation of model weights. This is a particular concern due to the sparse station temperature data used for model training, which could lead to overfitting in pixels with station observations and cause areas of differing predictions to surrounding grid cells.

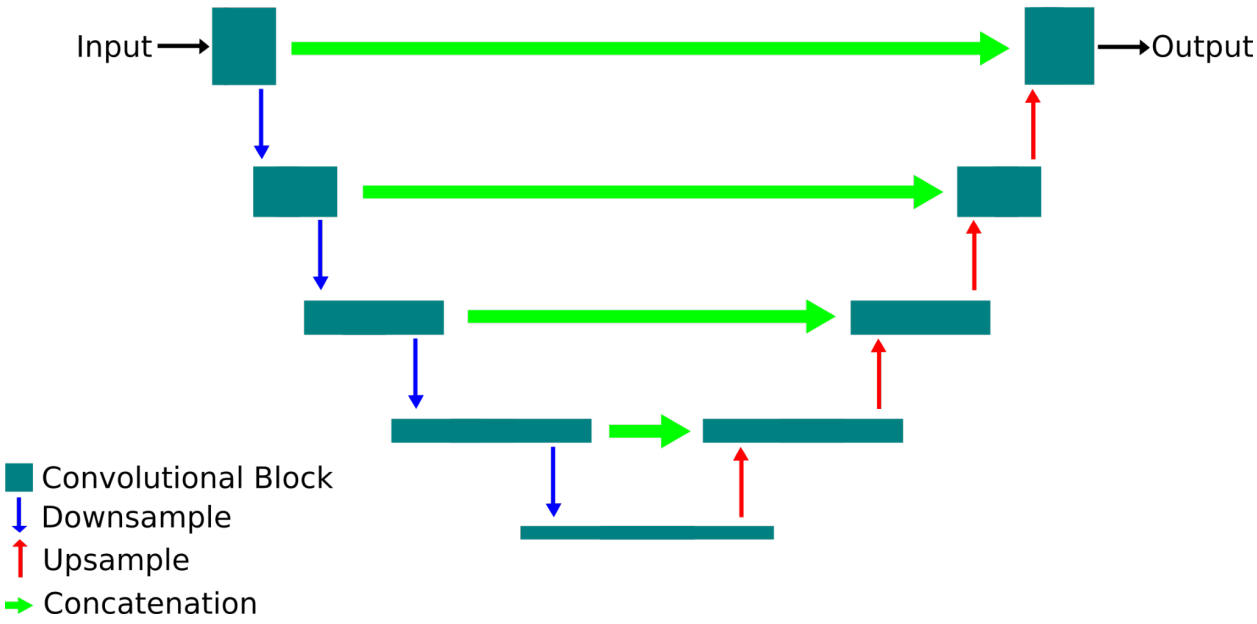

Figure 5: *U-Net model diagram. Dark green polygons represent convolutional blocks, blue arrows represent downsample operations, red arrows represent upsample operations, and green arrows represent concatenation operations.*

Model training and verification were done using data from the years 2017, 2018, and 2019; whereas, model validation was done against independent observations from years 2016 and 2020. After each epoch the model was verified against observational data from a selection of model training years, and the model with the highest performance score was saved as the final model. Scoring was done using the Matthews Correlation Coefficient (MCC). MCC accounts for true and false positives and negatives when evaluating the model outputs and works even if there is a large class imbalance. The MCC can be calculated using the formula:

$$MCC = \frac{TP\ x\ TN - FPxFN}{\sqrt{(TP+FP)(TP+FN)(TN+FP)(TN+FN)}}, \quad (2)$$

where TP is the number of true positives, TN is the number of true negatives, FP is the number of false positives, and FN is the number of false negatives.

6 - Data Format

The data are provided in individual multi-layer GeoTIFF files for each daily granule in the product time series; where each daily file includes both probabilistic (band 1) and binary (band 2) FT granules. To reduce file size, the product data values are stored as shorts that must be divided by 10,000 to convert back to the original floating point data.

This provides a roughly 50% reduction in file size when stored using this method. Once converted back to the original floating point data the data values are defined as follows (Table 1). Separate data files are included for morning (AM) and afternoon (PM) conditions as defined by the satellite overpasses and depicted in the file names.

Table 1. FT variable definitions.

Classification	value
Frozen (binary)	0
Thawed (binary)	1
Thawed probability (low [0] to high [1])	Range: 0-1
Water dominated pixel	-1
Ice dominated pixel	-2
Missing data	-3

Each daily file is projected in the same Northern-Hemisphere Polar EASE-Grid 2 projection format with 9km resolution gridding and 2000x2000 pixels over the domain. The geographical range of the product is the Northern Hemisphere, with -180° to 180° longitudinal coverage and extending from 0° to 90°- latitude.

7 - Data Organization

The data are stored in a hierarchical file structure by year of record from 2016 through 2020. Each daily file is saved using the naming format: *NH_PROBABILISTIC_[AM or PM]_FT_[year]_day[3 digit day of year].tif and ranging* from January first (DOY 001) to December 31st (DOY 365). The uncompressed individual file sizes are 15.27 MB, while the total multi-year data record is 55.89GB. The entire archive is also available as a compressed zip file (~2.46GB) for more efficient download and storage.

8 - References

“ASSIMO Project.” n.d. Accessed May 5, 2022. http://assimo.meteoromania.ro.

Beyrich, Frank, and Wolfgang K. Adam. 2007. *Site and Data Report for the Lindenberg Reference Site in CEOP - Phase I*. Selbstverlag des Deutschen Wetterdienstes.

Bircher, S., N. Skou, K. H. Jensen, J. P. Walker, and L. Rasmussen. 2012. “A Soil Moisture and Temperature Network for SMOS Validation in Western Denmark.” *Hydrology and Earth System Sciences*. https://doi.org/10.5194/hess-16-1445-2012.

Bogena, Heye, Ralf Kunkel, Thomas Pütz, Harry Vereecken, Elisabeth Krüger, Steffen Zacharias, Peter Dietrich, et al. 2012. “TERENO - Long-Term Monitoring Network for

Terrestrial Environmental Research." *Hydrologie Und Wasserbewirtschaftung*, Hydrologie und Wasserbewirtschaftung (HyWa), 56 (3): 138–43.

Brodzik, Mary J., Brendan Billingsley, Terry Haran, Bruce Raup, and Matthew H. Savoie. 2014. "Correction: Brodzik, MJ, et Al. EASE-Grid 2.0: Incremental but Significant Improvements for Earth-Gridded Data Sets. ISPRS International Journal of Geo-Information 2012, 1, 32--45." *ISPRS International Journal of Geo-Information* 3 (3): 1154–56.

Brodzik, Mary J., David G. Long, and Molly A. Hardman. 2021. "SMAP Radiometer Twice-Daily rSIR-Enhanced EASE-Grid 2.0 Brightness Temperatures, Version 2." NASA National Snow and Ice Data Center DAAC. https://doi.org/10.5067/YAMX52BXFL10.

Brodzik, M. J., and NSIDC. 2013. "EASE-Grid 2.0 Land-Ocean-Coastline-Ice Masks Derived from Boston University Global MODIS/Terra Land Cover Data." NASA National Snow and Ice Data Center DAAC. https://doi.org/10.5067/VY2JQZL9J8AQ.

Brown, Jordan P., and David G. Long. 2022. "Resolution Enhancement of SMAP Passive Soil Moisture Estimates." *Remote Sensing* 14 (7): 1761.

Calvet, Jean-Christophe, Noureddine Fritz, Francis Froissard, David Suquia, Alain Petitpa, and Bruno Piguet. 2007. "In Situ Soil Moisture Observations for the CAL/VAL of SMOS: The SMOSMANIA Network." In *2007 IEEE International Geoscience and Remote Sensing Symposium*, 1196–99.

Derksen, Chris, Xiaolan Xu, R. Scott Dunbar, Andreas Colliander, Youngwook Kim, John S. Kimball, T. Andrew Black, et al. 2017. "Retrieving Landscape Freeze/thaw State from Soil Moisture Active Passive (SMAP) Radar and Radiometer Measurements." *Remote Sensing of Environment* 194 (June): 48–62.

Dorigo, Wouter, Irene Himmelbauer, Daniel Aberer, Lukas Schremmer, Ivana Petrakovic, Luca Zappa, Wolfgang Preimesberger, et al. 2021. "The International Soil Moisture Network: Serving Earth System Science for over a Decade." *Hydrology and Earth System Sciences* 25 (11): 5749–5804.

Farhadi, Leila, Rolf H. Reichle, Gabriëlle J. M. De Lannoy, and John S. Kimball. 2015. "Assimilation of Freeze–Thaw Observations into the NASA Catchment Land Surface Model." *Journal of Hydrometeorology* 16 (2): 730–43.

"Global Learning and Observations to Benefit the Environment (GLOBE) Program." n.d. Accessed September 24, 2021. https://www.globe.gov/globe-data.

González-Zamora, Á., N. Sánchez, M. Pablos, and J. Martínez-Fernández. 2019. "CCI Soil Moisture Assessment with SMOS Soil Moisture and in Situ Data under Different Environmental Conditions and Spatial Scales in Spain." *Remote Sensing of Environment* 225 (May): 469–82.

GTN-P. 2015. "Global Terrestrial Network for Permafrost Metadata for Permafrost Boreholes (TSP) and Active Layer Monitoring (CALM) Sites, Supplement to: Biskaborn, Boris K; Lanckman, Jean-Pierre; Lantuit, Hugues; Elger, Kirsten; Streletskiy, Dmitry A; Cable, William L; Romanovsky, Vladimir E (2015): The New Database of the Global Terrestrial Network for Permafrost (GTN-P). Earth System Science Data, 7(2), 245-259." PANGAEA - Data Publisher for Earth & Environmental Science. https://doi.org/10.1594/PANGAEA.842821.

Hersbach, Hans, Bill Bell, Paul Berrisford, Shoji Hirahara, András Horányi, Joaquín Muñoz-Sabater, Julien Nicolas, et al. 2020. "The ERA5 Global Reanalysis." *Quarterly Journal of the Royal Meteorological Society* 146 (730): 1999–2049.

Ikonen, J., J. Vehviläinen, K. Rautiainen, T. Smolander, J. Lemmetyinen, S. Bircher, and J. Pulliainen. n.d. “The Sodankylä in-Situ Soil Moisture Observation Network: An Example Application to Earth Observation Data Product Evaluation.” https://doi.org/10.5194/gid-5-599-2015.

JAXA. n.d. “G-PortalTop.” Accessed May 3, 2022. https://gportal.jaxa.jp/gpr/.

Kim, Youngwook, John Kimball, Joe Glassy, and Kyle McDonald. 2021. “MEaSUREs Northern Hemisphere Polar EASE-Grid 2.0 Daily 6 Km Land Freeze/thaw Status from AMSR-E and AMSR2, Version 2.” NASA National Snow and Ice Data Center DAAC. https://doi.org/10.5067/BDY2V548E07C.

Kim, Youngwook, John S. Kimball, and Jinyang Du. 2017. “Satellite Microwave Remote Sensing of Landscape Freeze--Thaw Status Related to Frost Hazard Monitoring.” In *Remote Sensing of Hydrometeorological Hazards*, 157–82. CRC Press.

Kim, Youngwook, John S. Kimball, Joseph Glassy, and Jinyang Du. 2017. “An Extended Global Earth System Data Record on Daily Landscape Freeze–thaw Status Determined from Satellite Passive Microwave Remote Sensing.” *Earth System Science Data*. https://doi.org/10.5194/essd-9-133-2017.

Kim, Youngwook, John S. Kimball, Xiaolan Xu, R. Scott Dunbar, Andreas Colliander, and Chris Derksen. 2019. “Global Assessment of the SMAP Freeze/Thaw Data Record and Regional Applications for Detecting Spring Onset and Frost Events.” *Remote Sensing*. https://doi.org/10.3390/rs11111317.

McDonald, Kyle C., and John S. Kimball. 2005. “Estimation of Surface Freeze-Thaw States Using Microwave Sensors.” In *Encyclopedia of Hydrological Sciences*. Chichester, UK: John Wiley & Sons, Ltd. https://doi.org/10.1002/0470848944.hsa059a.

McGlinchy, Joe, Brian Johnson, Brian Muller, Maxwell Joseph, and Jeremy Diaz. 2019. “Application of UNet Fully Convolutional Neural Network to Impervious Surface Segmentation in Urban Environment from High Resolution Satellite Imagery.” In *IGARSS 2019 - 2019 IEEE International Geoscience and Remote Sensing Symposium*, 3915–18.

Musial, J. P., Katarzyna Dabrowska-Zielinska, Wojciech Kiryla, Ryszard Oleszczuk, Tomasz Gnatowski, and Jacek Jaszczynski. 2016. “Derivation and Validation of the High Resolution Satellite Soil Moisture Products: A Case Study of the Biebrza Sentinel-1 Validation Sites.” *Issues* 8: 37–53.

“NVE.” n.d. Accessed May 5, 2022. https://www.nve.no/hydrology/?ref=mainmenu.

Petropoulos, George P., and Jon P. McCalmont. 2017. “An Operational In Situ Soil Moisture & Soil Temperature Monitoring Network for West Wales, UK: The WSMN Network.” *Sensors* 17 (7). https://doi.org/10.3390/s17071481.

Qamar, Saqib, Hai Jin, Ran Zheng, Parvez Ahmad, and Mohd Usama. 2020. “A Variant Form of 3D-UNet for Infant Brain Segmentation.” *Future Generations Computer Systems: FGCS* 108 (July): 613–23.

Ronneberger, Olaf, Philipp Fischer, and Thomas Brox. 2015. “U-Net: Convolutional Networks for Biomedical Image Segmentation.” In *Medical Image Computing and Computer-Assisted Intervention – MICCAI 2015*, 234–41. Springer International Publishing.

Tompson, Jonathan, Ross Goroshin, Arjun Jain, Yann LeCun, and Christopher Bregler. 2014. “Efficient Object Localization Using Convolutional Networks.” *arXiv [cs.CV]*. arXiv. http://arxiv.org/abs/1411.4280.

Ulmas, Priit, and Innar Liiv. 2020. “Segmentation of Satellite Imagery Using U-Net Models for Land Cover Classification.” *arXiv [cs.CV]*. arXiv. http://arxiv.org/abs/2003.02899.

USDA Natural Resources Conservation Service. 2017. “National Water and Climate Center Interactive Map.” *USDA National Water and Climate Center*. https://data.nal.usda.gov/dataset/national-water-and-climate-center-interactive-map.

Varlagin, Andrej. n.d. “Ru_CFR.”

Vreugdenhil, M., W. Dorigo, M. Broer, P. Haas, A. Eder, P. Hogan, G. Bloeschl, and W. Wagner. 2013. “Towards a High-Density Soil Moisture Network for the Validation of SMAP in Petzenkirchen, Austria.” In *2013 IEEE International Geoscience and Remote Sensing Symposium - IGARSS*, 1865–68.

Wigneron, Jean-Pierre, Sylvia Dayan, Alain Kruszewski, Christelle Aluome, Marie Guillot-Ehret Amen Al-Yaari, Lei Fan, Serhat Guven, et al. 2018. “The Aqui Network: Soil Moisture Sites in the ‘Les Landes’ Forest and Graves Vineyards (Bordeaux Aquitaine Region, France).” In *IGARSS 2018 - 2018 IEEE International Geoscience and Remote Sensing Symposium*, 3739–42.

Xu, Xiaolan, R. Scott Dunbar, Chris Derksen, Andreas Colliander, Youngwook Kim, and John Kimball. 2020. “SMAP Enhanced L3 Radiometer Global and Northern Hemisphere Daily 9 Km EASE-Grid Freeze/thaw State, Version 3.” NASA National Snow and Ice Data Center DAAC. https://doi.org/10.5067/ZV08T8J395JB.

Zwieback, Simon, Annett Bartsch, Thomas Melzer, and Wolfgang Wagner. 2011. “Probabilistic Fusion of $$\hbox {K}$ \_ ${$$\rm U} -and C-Band Scatterometer Data for Determining the Freeze/Thaw State.” *IEEE Transactions on Geoscience and Remote Sensing: A Publication of the IEEE Geoscience and Remote Sensing Society* 50 (7): 2583–94.